Proceedings of the ASME 2020
International Design Engineering Technical Conferences
and Computers and Information in Engineering Conference
IDETC/CIE2020
August 17-19, 2020, Virtual, Online

DETC2020-22145

ELECTROMECHANICAL DIODE: ACOUSTIC NON-RECIPROCITY IN WEAKLY NONLINEAR METAMATERIAL WITH ELECTROMECHANICAL RESONATORS

Mohammad A. Bukhari
Department of Mechanical Engineering
Virginia Tech, Blacksburg, Virginia 24061
Email: bukhari@vt.edu

Oumar R. Barry*
Department of Mechanical Engineering
Virginia Tech, Blacksburg, Virginia 24061
Email: obarry@vt.edu

ABSTRACT

Recent attention has been given to acoustic non-reciprocity in metamaterials with nonlinearity. However, the study of asymmetric cells has been limited to mechanical diodes only. There is no work reported on electromechanical rectifiers or diodes. This problem is investigated here by analytically and numerically studying a combination of nonlinear and linear chains coupled with electromechanical resonators. The system is simulated numerically using MATLAB built in integrator and the results are validated by results found in the literature. Numerical examples are carried out to obtain band structure, operation range of electromechanical diode, harvested power, and significant frequency shift, which is demonstrated using spectro-spatial analyses. The observed frequency shift is used to construct an electromechanical diode to guide the wave to propagate in one direction only. This only allows signal sensing for waves propagating in one direction and rejects any other signals. Furthermore, this electromechanical diode is evaluated by calculating the transmission ratio and the asymmetric ratio for a transient input signal.

INTRODUCTION

The study of metamaterials has recently received considerable attention. Metamaterials are artificially engineered materials built in special configurations and with special constituents. These materials have unique dynamic properties in many engineering applications (e.g., vibration attenuation, cloaking, and wave focusing). These properties cannot be found in homogeneous materials [1, 2].

When metamaterials are represented by periodic cells, they are often called phononic crystals [3–8]. Arranging periodic cells carefully can mitigate travelling waves with a wavelength close to their lattice constants due to Bragg scattering. The lattice size constraint in periodic structures restricts the applications to vibration control of large structures.

Controlling smaller size structures can be achieved with locally resonant metamaterials [9]. These metamaterials are fabricated by embedding local resonators inside the structure. The resulting structure can mitigate waves with wavelengths much larger than the lattice constant. Note that periodicity is not essential in locally resonant metamaterials since the resonance mode would hybridize with the long-wave nondispersive modes of the underlying medium for low resonator frequency. Consequently, a band gap may be generated without the need for Bragg scattering [10]. The transition between Brag scattering and mode hybridization in locally resonant metamaterial can be found in [11].

In addition to the unique dynamic property offered by metamaterials for vibration mitigation applications, nonlinear metamaterials exhibit other dynamic properties that show interesting wave propagation phenomena. These phenomena include gap solitons [12], dark solitons, envelope and dark solitons [13], cloaking [14], acoustic non-reciprocity [15], and tuned bandgap limits [16].

Nonlinear metamaterials are usually analyzed analytically or numerically. The nature of the former depends significantly on the type of nonlinearity. Weakly nonlinear systems can by ana-

*Address all correspondence to this author.

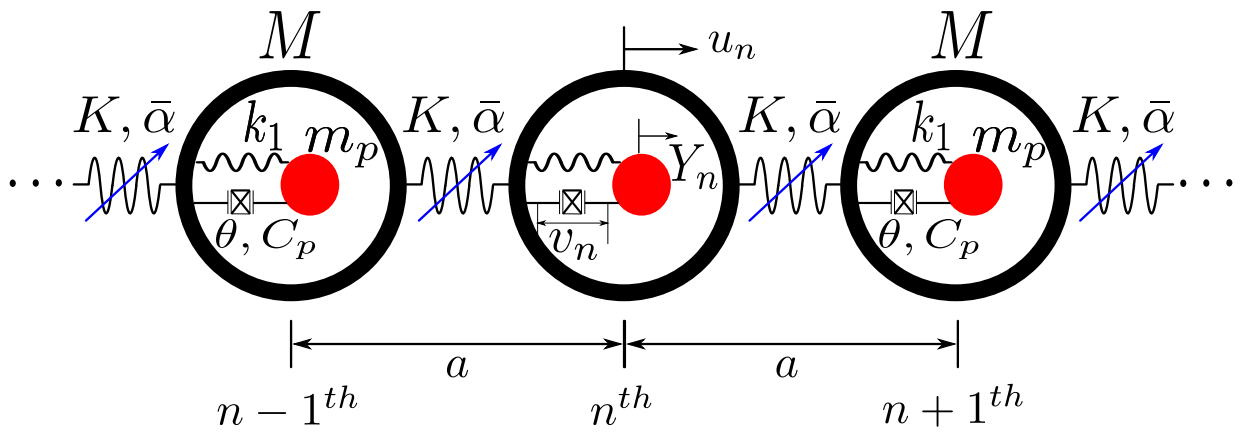

FIGURE 1: A schematic diagram for the nonlinear acoustic metamaterial with electromechanical resonators

lyzed using perturbation techniques [17, 18]. Examples of nonlinear metamaterials can be found in [19] for nonlinear chains, [20] for locally resonant metamaterials, and [21–23] for nonlinear chains with multiple linear and nonlinear local resonators. In addition to weakly nonlinear metamaterials, Abedin-Nasab et al., have investigated dispersion relations for strongly nonlinear metamaterials using homotopy analysis [24]. Metamaterials can also be analyzed by different numerical techniques. The numerical results can further be analyzed using spectro-spatial analyses to demonstrate other nonlinear wave propagation features that cannot be captured from the dispersion curves [20,22,23,25,26].

In addition to the mechanical bandgap, many investigators have studied the electromechanical bandgap by attaching piezoelectric patches to periodic structures. These piezoelectric patches add a stiffness to the structure due to the electromechanical coupling; therefore, they can control the size of the generated bandgap [27–31]. Moreover, these embedded piezoelectric materials can be employed for harvesting power simultaneously with vibration attenuation. This is motivated by the flat band of frequencies observed in metamaterials [32–36]. The application of metamaterials with piezoelectric patches is not limited to vibration suppression and energy harvesting. In fact, they can also be utilized in wave focusing in 2D metamaterials for enhancing energy harvesting [37]. Furthermore, the study of nonlinear metamaterials with electromechanical resonators can be found in [26]. Bukhari and Barry [26] have shown that solitary waves can enhance the energy harvested by electromechanical resonators. They also demonstrated analytically and numerically that electromechanical coupling in resonators has no effect on the size of the bandgap and only nonlinearity can alter the band structure.

Waves propagating in nonlinear metamaterials can be distorted based on the wave's amplitude and wavelength. This distortion usually results in a frequency shift for the wave components; therefore, some of the energy content can appear at frequencies different from the input frequency. Coupling the nonlinear metamaterial with a linear metamaterial (i.e., the linear metamaterial has a bandgap tuned to the region of frequency shift in the nonlinear metamaterial) results in wave non-reciprocity [15, 38–41]. This restricts the wave to only propagate in unidirection (e.g., acoustic rectifier or diode). Acoustic rectifiers can also be constructed by granular structures [40] or nonlinear hierarchical internal structures [42]. Models of acoustic diodes were limited to the use of local mechanical resonators embedded within the periodic structure or simple coupling between linear and nonlinear metamaterials. To the best of our knowledge, there are no models in the literature investigating the use of electromechanical resonators in nonlinear metamaterials for designing electromechanical diodes. This is the focus of the current study.

In this paper, we examine a weakly nonlinear metamaterial with electromechanical local resonators. The nonlinearity stems from the chain and is of a cubic type. The system is simulated numerically and validated against other models in the literature. The numerical results are used to obtain the band structures and analyzed further by spectro-spatial analyses to demonstrate the frequency shift in the nonlinear chain. This frequency shift is then used to design an electromechanical diode. The designed electromechanical diode is evaluated based on its transmission ratio and the asymmetric ratio for a transient input signal.

SYSTEM DESCRIPTION AND MATHEMATICAL MODELING

A schematic diagram for the metamaterial chain with electromechanical resonators is shown in Fig. 1. The chain is constructed of s periodic cells with a mass, M, lattice constant, a, and connected by a weakly nonlinear spring. The springs have linear coefficient, K, and nonlinear coefficient $\bar{\alpha}$. Attached to each cell, there is a local electromechanical resonator shunted to an external resistor R. The electromechanical resonator has effective mass, m_p, effective stiffness, k_1, electromechanical cou-

pling coefficient, θ, and capacitance of the piezoelectric element, C_p. It is noteworthy here that the system is reduced to a linear system when $\bar{\alpha} = 0$.

The equation of motions for the n^{th} cell and its electromechanical resonator can be expressed as follows

$$\begin{aligned} M\ddot{\bar{u}}_n + 2K\bar{u}_n - K\bar{u}_{n+1} - K\bar{u}_{n-1} + \bar{\alpha}(\bar{u}_n - \bar{u}_{n+1})^3 + \\ \bar{\alpha}(\bar{u}_n - \bar{u}_{n-1})^3 + m_p(\ddot{\bar{y}}_n + \ddot{\bar{u}}_n) = 0 \end{aligned} \tag{1}$$

$$m_p\ddot{\bar{y}}_n + k_1\bar{y}_n - \theta\bar{v}_n = -m_p\ddot{\bar{u}}_n \tag{2}$$

$$RC_p\dot{\bar{v}}_n + \bar{v}_n + R\theta\dot{\bar{y}}_n = 0 \tag{3}$$

where $\bar{u}_n$ is the displacement of the n^{th} cell, $\bar{y}_n = Y_n - \bar{u}_n$ is the net displacement of the n^{th} electromechanical resonator, Y_n is the absolute displacement of the electromechanical resonator, $\bar{v}_n$ is the harvested voltage in the n^{th} electromechanical resonator, and the dots are the derivative with respect to time.

We introduce the following dimensionless parameters in order to normalize Eqns. (1)-(3):

$$\begin{aligned} \omega_n^2 = K/M, \omega_d^2 = k_1/m_p, \bar{k} = k_1/K, u_n = \bar{u}_n/U_0, \\ y_n = \bar{y}_n/y_0, v_n = \bar{v}_n/V_0, \alpha = \bar{\alpha}U_0^2/K, \Omega_0 = \omega_n/\omega_d, \\ \alpha_1 = \theta V_0/k_1, \alpha_2 = RC_p\omega_n, \alpha_3 = R\theta\omega_n y_0/V_0, \tau = \omega_n t \end{aligned} \tag{4}$$

where U_0, V_0, y_0 are the zeroth cell displacement, harvested voltage, and resonator displacement, respectively.

Substituting Eqn. (4) into Eqns. (1)-(3) yields the following normalized equations

$$\begin{aligned} \ddot{u}_n + 2u_n - u_{n+1} - u_{n-1} + \alpha(u_n - u_{n+1})^3 + \\ \alpha(u_n - u_{n-1})^3 + \bar{k}\Omega_0^2(\ddot{y}_n + \ddot{u}_n) = 0 \end{aligned} \tag{5}$$

$$\Omega_0^2\ddot{y}_n + y_n - \alpha_1 v_n = -\Omega_0^2\ddot{u}_n \tag{6}$$

$$\alpha_2\dot{v}_n + v_n + \alpha_3\dot{y}_n = 0 \tag{7}$$

For weakly nonlinear system (i.e., assuming $\alpha = \varepsilon\alpha$), one can write the solution up to the second order expansion as

$$u_n(t,\varepsilon) = u_{n0}(T_0,T_1) + \varepsilon u_{n1}(T_0,T_1) + o(\varepsilon^2) \tag{8}$$

$$y_n(t,\varepsilon) = y_{n0}(T_0,T_1) + \varepsilon y_{n1}(T_0,T_1) + o(\varepsilon^2) \tag{9}$$

$$v_n(t,\varepsilon) = v_{n0}(T_0,T_1) + \varepsilon v_{n1}(T_0,T_1) + o(\varepsilon^2) \tag{10}$$

where $T_0 = \tau$ and $T_1 = \varepsilon\tau$ are the fast and slow time scales, respectively, while ε is a small dimensionless parameter.

For system with two time scales, the time derivative can be expressed as

$$(\dot{}) = D_0 + \varepsilon D_1 + ... \tag{11}$$

$$(\ddot{}) = D_0^2 + 2\varepsilon D_0 D_1 + ... \tag{12}$$

Substituting Eqns. (8)-(12) into Eqns. (5)-(7) and collecting the terms of similar coefficient at orders ε^0 and ε leads to

order ε^0

$$D_0^2 u_{n0} + 2u_{n0} - u_{(n-1)0} - u_{(n+1)0} + \bar{k}\Omega_0^2 D_0^2(y_{n0} + u_{n0}) = 0 \tag{13}$$

$$\Omega_0^2 D_0^2 y_{n0} + y_{n0} - \alpha_1 v_{n0} = -\Omega_0^2 D_0^2 u_{n0} \tag{14}$$

$$\alpha_2 D_0 v_{n0} + v_{n0} + \alpha_3 D_0 y_{n0} = 0 \tag{15}$$

order ε^1

$$\begin{aligned} D_0^2 u_{n1} + 2u_{n1} - u_{(n-1)1} - u_{(n+1)1} + \\ \bar{k}\Omega_0^2 D_0^2(y_{n1} + u_{n1}) = -2\bar{k}\Omega_0^2 D_0 D_1(y_{n0} + u_{n0}) - \\ 2D_0 D_1 u_{n0} - \alpha(u_{n0} - u_{(n-1)0})^3 - \alpha(u_{n0} - u_{(n+1)0})^3 \end{aligned} \tag{16}$$

$$\begin{aligned} \Omega_0^2 D_0^2 y_{n1} + y_{n1} - \alpha_1 v_{n1} = -\Omega_0^2 D_0^2 u_{n1} - 2\Omega_0^2 D_0 D_1 u_{n0} - \\ 2\Omega_0^2 D_0 D_1 y_{n0} \end{aligned} \tag{17}$$

$$\alpha_2 D_0 v_{n1} + v_{n1} + \alpha_3 D_0 y_{n1} = -\alpha_2 D_1 v_{n0} - \alpha_3 D_1 y_{n0} \tag{18}$$

LINEAR BANDGAP

For the linear problem (i.e., at order ε^0), the solution of the linear system can be defined as

$$u_n = Ae^{i(nk - \omega\tau)} \tag{19}$$

$$y_n = Be^{i(nk - \omega\tau)} \tag{20}$$

$$v_n = Ce^{i(nk - \omega\tau)} \tag{21}$$

Introducing Eqns. (19)-(21) into Eqns. (13)-(15) yields the following dispersion relation

$$-\omega^2 + (2 - 2\cos k) - \bar{k}\Omega_0^2\omega^2(1 + K_\omega) = 0 \tag{22}$$

where $K_\omega = \frac{\Omega_0^2\omega^2}{1 - \alpha_1\Gamma - \Omega_0^2\omega^2}$, and $\Gamma = \frac{i\alpha_3\omega}{1 - i\alpha_2\omega}$.

NONLINEAR BANDGAP

For nonlinear problem (i.e., ε), one can write the nonlinear frequency equation, following [26], as

$$\omega_{nl} = \omega - \varepsilon b' \tag{23}$$

where b' is the phase resulting from expressing A in the polar form (i.e., $A = ae^{ib}$) and is defined as

$$b' = c_1 a_0^2 \tag{24}$$

The constant c_1 is defined as

$$c_1 = -\frac{gl + mh}{h^2 + g^2} \tag{25}$$

where

$$\begin{aligned} g = -\frac{1}{2}\omega\big(\alpha_2\omega\big(\Omega_0^2\big(\bar{k}\,(\alpha_1(-\mathrm{Im}[\Gamma])\mathrm{Im}[K_\omega] + \\ (\alpha_1\mathrm{Re}[\Gamma] - 2)\,\mathrm{Re}[K_\omega] - 2) + 2\omega^2\big) - 2\big) + \\ 2\Omega_0^2\bar{k}\mathrm{Im}[K_\omega] - \alpha_1\alpha_3\omega\big(\Omega_0^2\bar{k}\,(\mathrm{Re}[K_\omega] + 2) + 2\big)\big) \end{aligned} \tag{26}$$

$$\begin{aligned} h = \frac{1}{2}\omega\big(\Omega_0^2\big(\bar{k}\,(\mathrm{Re}[K_\omega]\,(\alpha_1\alpha_2\mathrm{Im}[\Gamma]\omega - 2) + \\ \omega\mathrm{Im}[K_\omega]\,(\alpha_2\,(\alpha_1\mathrm{Re}[\Gamma] - 2) - \alpha_1\alpha_3) - 2) + 2\omega^2\big) - 2\big) \end{aligned} \tag{27}$$

$$f = \frac{3}{2}\alpha\mathrm{ccc}\left(\omega^2\Omega_0^2 - 1\right) \tag{28}$$

$$l = \frac{1}{2}(-3)\alpha\mathrm{ccc}\omega\left(\alpha_2\left(\omega^2\Omega_0^2 - 1\right) - \alpha_1\alpha_3\right) \tag{29}$$

ANALYTICAL AND NUMERICAL BANDGAPS

To check our analytical dispersion relations, we plot the analytical and numerical band structure of the system with electromechanical resonator in Fig. 2. The numerical simulations are carried out by simulating a chain with 500 cells. The parameters of the metamaterial with electromechanical resonator are chosen to be: $\bar{k} = 1$, $\omega_n = \omega_d = 1000$, $k_1 = 10^6$ N/M, $C_p = 13.3 \times 10^{-9}$ F, $R = 10^7\Omega$, and $\theta = 10^{-8}$ N/V. The system is excited by a transient wave packet and integrated numerically in MATLAB. To limit the propagation in one direction, we define the initial conditions as

$$\begin{aligned} u_m(0) = \frac{1}{2}(H(m-1) - H(m-1-N_{cy}2\pi/k))(1- \\ \cos(mk/N_{cy}))\sin(mk) \end{aligned} \tag{30}$$

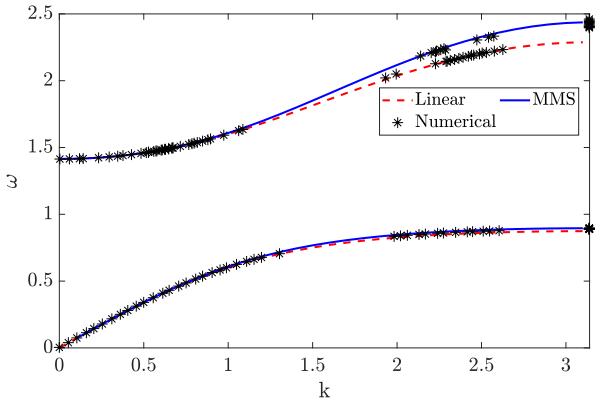

FIGURE 2: Band structure for linear and nonlinear metamaterials with electromechanical resonators obtained analytically and numerically.

$$\begin{aligned} \dot{u}_m(0) = \frac{1}{2}(H(m-1) - H(m-1-N_{cy}2\pi/k)) \\ (-\omega_n\omega/N_{cy}\sin(mk/N_{cy})\sin(mk) - \omega_n\omega(1- \\ \cos(mk/N_{cy}))\cos(mk)) \end{aligned} \tag{31}$$

$$y_m(0) = K_\omega u_m(0) \tag{32}$$

$$\dot{y}_m(0) = K_\omega \dot{u}_m(0) \tag{33}$$

$$v = \Gamma K_\omega u_m(0) \tag{34}$$

where $H(x)$ is the Heaviside function, and N_{cy} is the number of cycles and is chosen to be $N_{cy} = 7$ in this section.

Upon analyzing the simulation results by 2D Fast Fourier Transform (FFT), each point in the dispersion curves (frequency/wavenumber) belongs to the peak of 2D FFT. Then, the complete band structure can be obtained from sweeping the wavenumber over the first Brillouin zone at the acoustic and optical modes.

Figure. 2 depicts the linear and nonlinear analytical band structures and the nonlinear numerical band structure. The results demonstrate that hardening nonlinearity shifts the dispersion curves up as compared to the linear curves. Moreover, the numerical integration results also demonstrate that the analytical solution can predict the boundary of the band structure; however, the analytical solution cannot capture the significant frequency shift that is observed numerically at the medium wavelength limit in the optical mode. This frequency shift will be used to design our electromechanical resonator and will be discussed further using the spectro-spatial analyses in the next section.

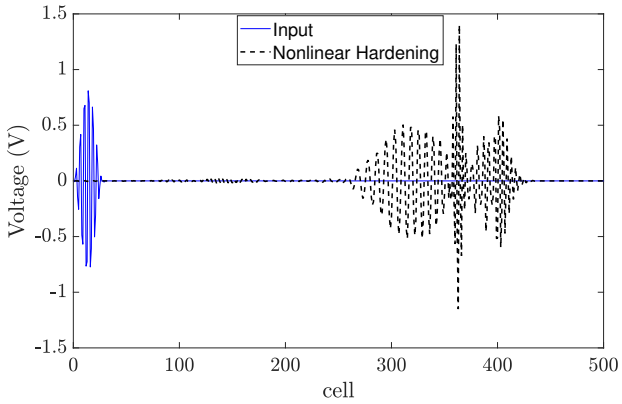

FIGURE 3: Spatial profile of the input/output voltage in the optical mode: $k = \pi/2$, $\varepsilon^2 A\Gamma = 0.03$.

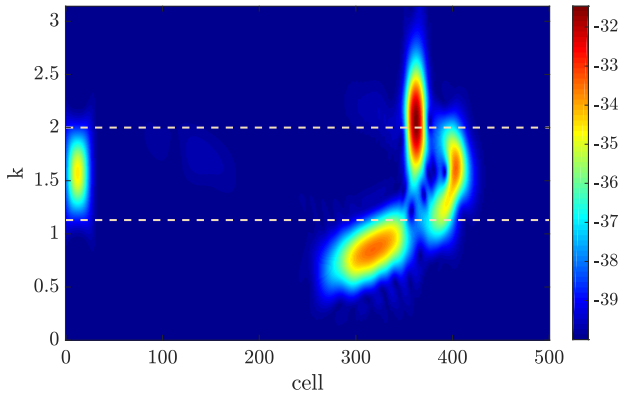

FIGURE 4: Spectrograms of the input/output voltage in the optical mode: $k = \pi/2$, $\varepsilon^2 A\Gamma = 0.03$.

SPECTRO-SPATIAL ANALYSES

To further demonstrate the significant frequency shift at the medium wavelength limit in the optical mode, we analyze the numerical results further by different signal processing techniques. First, we plot the spatial profile of the input and output voltage signals harvested by the electromechanical resonator at the end of the simulation in Fig. 3. The results indicate that the input signal is severely distorted and broken into several components. These components are: (1) a localized with high-amplitude wave (solitary wave), and (2) two stretched and low-amplitude waves (dispersive waves). This indicates that the output wave appears at different frequencies other than the input frequency.

These components are clearly demonstrated in Fig. 4, which shows the Short Term Fourier Transform (STFT) of the input/output signals' spatial components over time. We use a Hann window with the size of the input signal to contain the propagating wave. The results indicate that the output voltage signal is broken into three components. The first component appears at wavenumber/frequency above the input wavenumber/frequency window and it has the highest energy content. The second component appears inside the initial window and it has the lowest energy content. Finally, the third component is shifted below the initial window and its energy content is between the first and second components. Thus, most of the energy content of the input signal appears at output signal frequencies different than the input signal frequencies. This shows a good potential for using the proposed system to design an electromechanical diode.

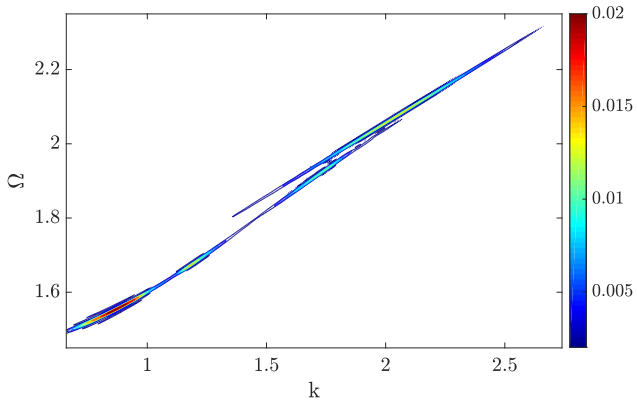

FIGURE 5: Contour plots of the 2D FFT of the output voltage in the optical mode: $k = \pi/2$, $\varepsilon^2 A\Gamma = 0.03$.

Further demonstration of the significant frequency shift in the system can be obtained by plotting the contour of 2D FFT for the output signal as shown in Fig. 5. The results also indicate that the output signal frequency components are distributed over a wide range of frequencies. Moreover, the high energy components are distributed over wavenumbers above and below the medium wavelength limit (i.e., wavelength of the input signal).

ELECTROMECHANICAL DIODE

Based on the significant frequency shift observed in the previous sections, we design an electromechanical diode for direction-biased waveguide applications. This diode allows waves to propagate in one direction; therefore, harvesting energy and sensing waves propagating in only one direction. A schematic diagram for the proposed electromechanical diode is shown in Fig. 6. The electromechanical diode is constructed from linear and nonlinear chains. The nonlinear chain with parameters defined above has a significant frequency region at medium wavelength limit in the optical mode. Any wave with frequency band in this region and propagating in the nonlinear chain appears at frequencies outside this region. The output signal can propagate into another linear chain with a bandgap tuned

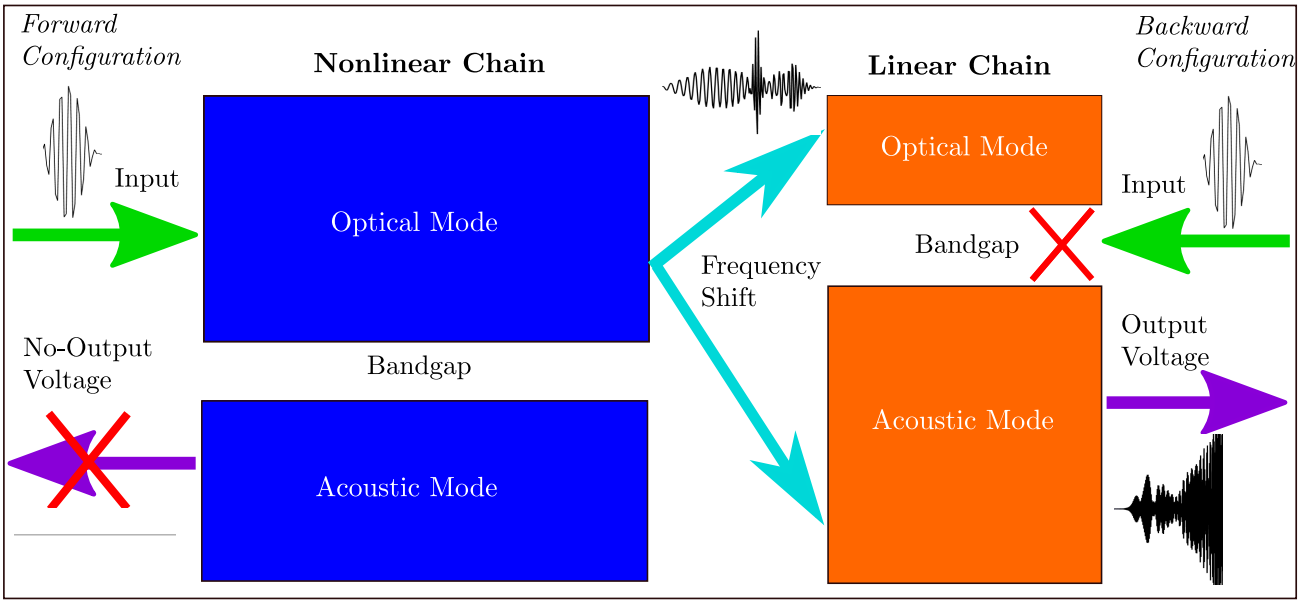

FIGURE 6: A schematic diagram for the electromechanical diode.

to the region of significant frequency shift in the nonlinear chain. Therefore, voltage can be harvested in the forward configuration. On the other hand, a wave with the same frequency band does not propagate when it excites the linear chain in the backward configuration. Therefore, voltage cannot be harvested in this configuration.

The combination of the linear and nonlinear chains constructing the electromechanical diode for forward and backward configurations is shown in Fig. 7. The nonlinear chain consists of 350 cells with the same parameters defined in the previous sections while the nonlinearity is chosen to be $\varepsilon^2 A\Gamma = 0.06$. The linear chain consists of 150 cells with parameters chosen to tune the chain bandgap to the significant frequency shift region in the nonlinear chain. These parameters are chosen as $\omega_n = 1000$ rad/sec, $\omega_d = 2034$ rad/sec, $k_1 = 164.3$ N/m, $\bar{k} = 0.127$, $C_p = 13.3 \times 10^{-9}$ F, $R = 10^7\Omega$, and $\theta = 10^{-10}$ N/V. It is noteworthy here that we chose the mass of the linear chain to be equal to the nonlinear chain mass to reduce the impedance mismatch.

We excite both configurations by a signal defined as

$$F_{ex} = \frac{1}{2}A[H(t) - H(t - \frac{2\pi\omega_n N_{cy}}{\omega\omega_d}][1 - cos(\frac{\omega_d\omega}{\omega_n N_{cy}}t)]sin(\frac{\omega_d\omega}{\omega_n}t) \tag{35}$$

where $N_{cy} = 60$.

For $\omega = 2$, voltage can be harvested at the other end in the forward configuration as shown in Fig. 8. However, the input wave cannot propagate in the backward configuration, thus no voltage can be harvested and the system acts as direction-biased waveguide as shown in Fig. 9. To evaluate the performance of the electromechanical diode, we need to calculate the input and output energy harvested in the 1^{st} and 500^{th} cells. The power can be determined as

$$P_n = \frac{V_n^2}{R} \tag{36}$$

In each configuration the transmission ratio can be determined as

$$Tr_f = \frac{\int_0^\tau P_{500}}{\int_0^\tau P_1} \tag{37}$$

$$Tr_b = \frac{\int_0^\tau P_1}{\int_0^\tau P_{500}} \tag{38}$$

where Tr_f and Tr_b are the transmission ratios for the forward and backward configurations, respectively. Upon calculating the transmission ratios for each configuration, the asymmetric ratio can be calculated as

$$\sigma = \frac{Tr_f}{Tr_b} \tag{39}$$

For forward configuration, the transmission ratio is $Tr_f = 61.57\%$. The achieved transmission ratio here in the forward

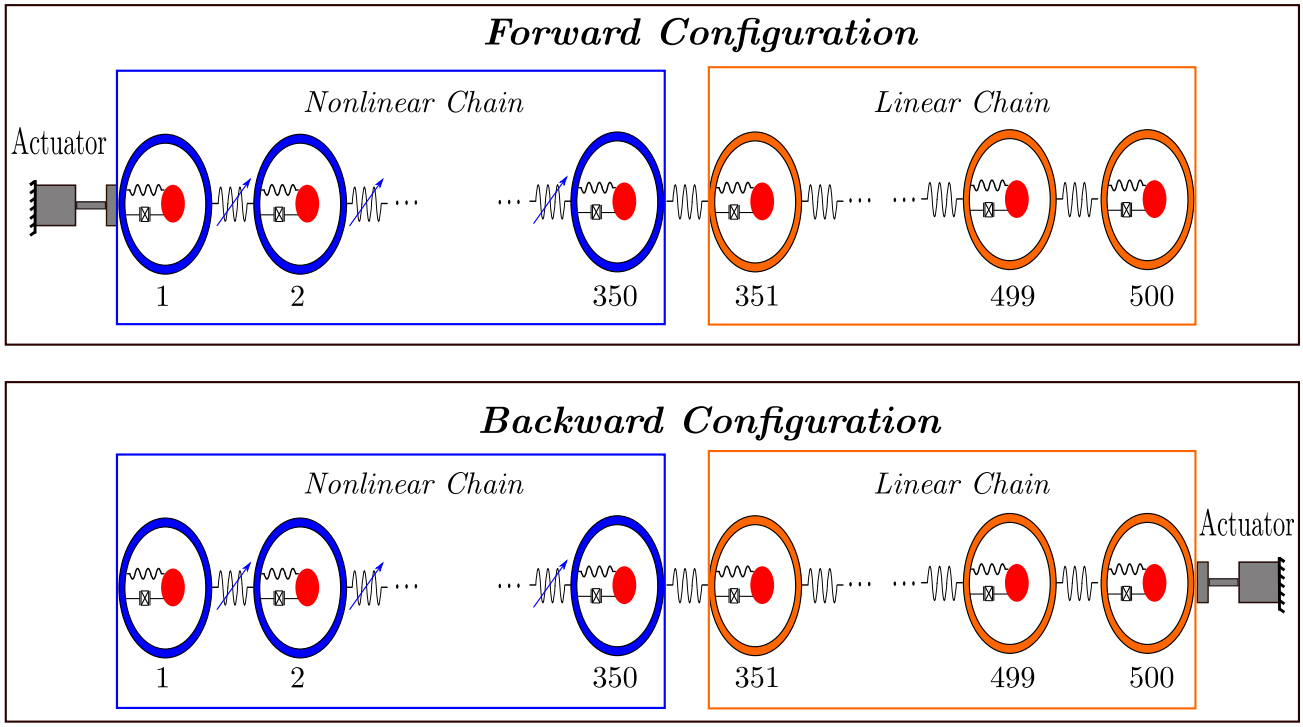

FIGURE 7: A schematic diagram for the forward and backward configurations.

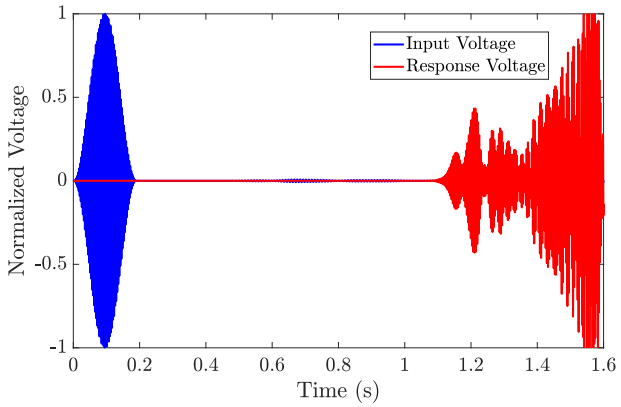

FIGURE 8: Input and output voltage harvested by the electromechanical resonator in the forward configuration.

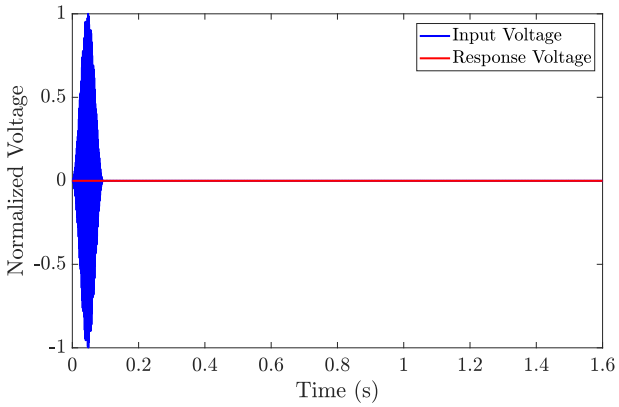

FIGURE 9: Input and output voltage harvested by the electromechanical resonator in the backward configuration.

configuration is high as compared to Ref. [15, 40]. The transmission ratio for the backward configuration is $Tr_b \approx 10^{-7}\%$. Moreover, the asymmetric ratio for the electromechanical diode is $\sigma \approx 6 \times 10^6$. These results show that the proposed electromechanical diode has a higher asymmetric ratio with higher transmission ratios than mechanical diodes reported in the literature. For instance, the asymmetric ratio in Refs. [15, 40] is $\sigma \approx 10^4$ and both reported low transmission ratios.

CONCLUSION

In this paper, a nonlinear metamaterial with electromechanical local resonators was investigated. The method of multiple scale was applied to the governing equations of motions to obtain the dispersion relations. The analytical band structure was validated via comparison with results obtained by direct numerical integration. The results indicated that the analytical results can predict the boundary of the band structure. However, the

analytical results cannot predict the dispersion curve at medium wavelength limit in the optical mode due to the significant frequency shift observed in this region. To further demonstrate the frequency shift in this region, we analyzed the numerical results by spectro-spatial analyses. The spatial profiles indicated that the wave is severely distorted in this region and split into localized and dispersive waves. Moreover, the spectrograms and contour plots of 2D FFT demonstrated that most of the energy content of the output voltage appears at frequencies outside the initial frequency band of the input signal. The observed significant frequency shift was utilized to design an electromechanical direction-biased waveguide (electromechanical diode). The proposed electromechanical diode was constructed by combining linear and nonlinear chains with electromechanical local resonators. This diode showed the ability to harvest energy and sense the wave propagating in the forward direction only and blocked any wave propagating in the backward configuration. Unlike mechanical diodes in the literature, the proposed diode does not only have a high asymmetric ratio, it also has a high transmission ratio for the forward configuration. Yet the proposed electromechanical diode can harvest energy and sense better than symmetric systems due to the birth of localized (solitary) waves.

ACKNOWLEDGMENT

This work was supported by the start-up grant provided by the Department of Mechanical Engineering at Virginia Tech.

REFERENCES

[1] Hussein, M. I., Leamy, M. J., and Ruzzene, M., 2014. "Dynamics of phononic materials and structures: Historical origins, recent progress, and future outlook". *Applied Mechanics Reviews,* ***66***(4), p. 040802.

[2] Bertoldi, K., Vitelli, V., Christensen, J., and van Hecke, M., 2017. "Flexible mechanical metamaterials". *Nature Reviews Materials,* ***2***(11), p. 17066.

[3] Sigalas, M. M., and Economou, E. N., 1992. "Elastic and acoustic wave band structure". *Journal of Sound Vibration,* ***158***, pp. 377–382.

[4] Sigalas, M., and Economou, E. N., 1993. "Band structure of elastic waves in two dimensional systems". *Solid state communications,* ***86***(3), pp. 141–143.

[5] Kushwaha, M. S., Halevi, P., Dobrzynski, L., and Djafari-Rouhani, B., 1993. "Acoustic band structure of periodic elastic composites". *Physical review letters,* ***71***(13), p. 2022.

[6] Kushwaha, M. S., Halevi, P., Martinez, G., Dobrzynski, L., and Djafari-Rouhani, B., 1994. "Theory of acoustic band structure of periodic elastic composites". *Physical Review B,* ***49***(4), p. 2313.

[7] Vasseur, J., Djafari-Rouhani, B., Dobrzynski, L., Kushwaha, M., and Halevi, P., 1994. "Complete acoustic band gaps in periodic fibre reinforced composite materials: the carbon/epoxy composite and some metallic systems". *Journal of Physics: Condensed Matter,* ***6***(42), p. 8759.

[8] Kushwaha, M. S., 1996. "Classical band structure of periodic elastic composites". *International Journal of Modern Physics B,* ***10***(09), pp. 977–1094.

[9] Liu, Z., Zhang, X., Mao, Y., Zhu, Y., Yang, Z., Chan, C. T., and Sheng, P., 2000. "Locally resonant sonic materials". *science,* ***289***(5485), pp. 1734–1736.

[10] Achaoui, Y., Laude, V., Benchabane, S., and Khelif, A., 2013. "Local resonances in phononic crystals and in random arrangements of pillars on a surface". *Journal of Applied Physics,* ***114***(10), p. 104503.

[11] Liu, L., and Hussein, M. I., 2012. "Wave motion in periodic flexural beams and characterization of the transition between bragg scattering and local resonance". *Journal of Applied Mechanics,* ***79***(1), p. 011003.

[12] Kivshar, Y. S., and Flytzanis, N., 1992. "Gap solitons in diatomic lattices". *Physical Review A,* ***46***(12), p. 7972.

[13] Nadkarni, N., Daraio, C., and Kochmann, D. M., 2014. "Dynamics of periodic mechanical structures containing bistable elastic elements: From elastic to solitary wave propagation". *Physical Review E,* ***90***(2), p. 023204.

[14] Darabi, A., Zareei, A., Alam, M.-R., and Leamy, M. J., 2018. "Experimental demonstration of an ultrabroadband nonlinear cloak for flexural waves". *Physical review letters,* ***121***(17), p. 174301.

[15] Liang, B., Yuan, B., and Cheng, J.-c., 2009. "Acoustic diode: Rectification of acoustic energy flux in one-dimensional systems". *Physical review letters,* ***103***(10), p. 104301.

[16] Manimala, J. M., and Sun, C., 2016. "Numerical investigation of amplitude-dependent dynamic response in acoustic metamaterials with nonlinear oscillators". *The Journal of the Acoustical Society of America,* ***139***(6), pp. 3365–3372.

[17] Nayfeh, A. H., 2011. *Introduction to perturbation techniques*. John Wiley & Sons.

[18] Nayfeh, A. H., and Mook, D. T., 2008. *Nonlinear oscillations*. John Wiley & Sons.

[19] Narisetti, R. K., Leamy, M. J., and Ruzzene, M., 2010. "A perturbation approach for predicting wave propagation in one-dimensional nonlinear periodic structures". *Journal of Vibration and Acoustics,* ***132***(3), p. 031001.

[20] Zhou, W., Li, X., Wang, Y., Chen, W., and Huang, G., 2018. "Spectro-spatial analysis of wave packet propagation in nonlinear acoustic metamaterials". *Journal of Sound and Vibration,* ***413***, pp. 250–269.

[21] Bukhari, M., and Barry, O., 2020. "Nonlinear metamaterials with multiple local mechanical resonators: Analytical and numerical analyses". In *New Trends in Nonlinear Dy-*

namics. Springer, pp. 13–21.

[22] Bukhari, M. A., and Barry, O. R. "On the spectro-spatial wave features in nonlinear metamaterials with multiple local resonators". In ASME 2019 International Design Engineering Technical Conferences and Computers and Information in Engineering Conference, American Society of Mechanical Engineers Digital Collection.

[23] Bukhari, M., and Barry, O., 2020. "Spectro-spatial analyses of a nonlinear metamaterial with multiple nonlinear local resonators". *Nonlinear Dynamics,* ***99***(2), pp. 1539–1560.

[24] Abedin-Nasab, M. H., Bastawrous, M. V., and Hussein, M. I., 2020. "Explicit dispersion relation for strongly nonlinear flexural waves using the homotopy analysis method". *Nonlinear Dynamics,* ***99***(1), pp. 737–752.

[25] Ganesh, R., and Gonella, S., 2013. "Spectro-spatial wave features as detectors and classifiers of nonlinearity in periodic chains". *Wave Motion,* ***50***(4), pp. 821–835.

[26] Bukhari, M., and Barry, O., 2020. "Simultaneous energy harvesting and vibration control in a nonlinear metastructure: A spectro-spatial analysis". *Journal of Sound and Vibration*, p. 115215.

[27] Thorp, O., Ruzzene, M., and Baz, A., 2001. "Attenuation and localization of wave propagation in rods with periodic shunted piezoelectric patches". *Smart Materials and Structures,* ***10***(5), p. 979.

[28] Airoldi, L., and Ruzzene, M., 2011. "Wave propagation control in beams through periodic multi-branch shunts". *Journal of Intelligent Material Systems and Structures,* ***22***(14), pp. 1567–1579.

[29] Casadei, F., Delpero, T., Bergamini, A., Ermanni, P., and Ruzzene, M., 2012. "Piezoelectric resonator arrays for tunable acoustic waveguides and metamaterials". *Journal of Applied Physics,* ***112***(6), p. 064902.

[30] Bergamini, A., Delpero, T., Simoni, L. D., Lillo, L. D., Ruzzene, M., and Ermanni, P., 2014. "Phononic crystal with adaptive connectivity". *Advanced Materials,* ***26***(9), pp. 1343–1347.

[31] Zhou, W., Wu, Y., and Zuo, L., 2015. "Vibration and wave propagation attenuation for metamaterials by periodic piezoelectric arrays with high-order resonant circuit shunts". *Smart Materials and Structures,* ***24***(6), p. 065021.

[32] Hu, G., Tang, L., Banerjee, A., and Das, R., 2017. "Metastructure with piezoelectric element for simultaneous vibration suppression and energy harvesting". *Journal of Vibration and Acoustics,* ***139***(1), p. 011012.

[33] Hu, G., Tang, L., and Das, R., 2017. "Metamaterial-inspired piezoelectric system with dual functionalities: energy harvesting and vibration suppression". In Active and Passive Smart Structures and Integrated Systems 2017, Vol. 10164, International Society for Optics and Photonics, p. 101641X.

[34] Hu, G., Tang, L., and Das, R., 2018. "Internally coupled metamaterial beam for simultaneous vibration suppression and low frequency energy harvesting". *Journal of Applied Physics,* ***123***(5), p. 055107.

[35] Shen, L., Wu, J. H., Zhang, S., Liu, Z., and Li, J., 2015. "Low-frequency vibration energy harvesting using a locally resonant phononic crystal plate with spiral beams". *Modern Physics Letters B,* ***29***(01), p. 1450259.

[36] Li, Y., Baker, E., Reissman, T., Sun, C., and Liu, W. K., 2017. "Design of mechanical metamaterials for simultaneous vibration isolation and energy harvesting". *Applied Physics Letters,* ***111***(25), p. 251903.

[37] Tol, S., Degertekin, F., and Erturk, A., 2017. "Phononic crystal luneburg lens for omnidirectional elastic wave focusing and energy harvesting". *Applied Physics Letters,* ***111***(1), p. 013503.

[38] Liang, B., Guo, X., Tu, J., Zhang, D., and Cheng, J., 2010. "An acoustic rectifier". *Nature materials,* ***9***(12), p. 989.

[39] Li, X.-F., Ni, X., Feng, L., Lu, M.-H., He, C., and Chen, Y.-F., 2011. "Tunable unidirectional sound propagation through a sonic-crystal-based acoustic diode". *Physical review letters,* ***106***(8), p. 084301.

[40] Boechler, N., Theocharis, G., and Daraio, C., 2011. "Bifurcation-based acoustic switching and rectification". *Nature materials,* ***10***(9), p. 665.

[41] Ma, C., Parker, R. G., and Yellen, B. B., 2013. "Optimization of an acoustic rectifier for uni-directional wave propagation in periodic mass–spring lattices". *Journal of Sound and Vibration,* ***332***(20), pp. 4876–4894.

[42] Moore, K. J., Bunyan, J., Tawfick, S., Gendelman, O. V., Li, S., Leamy, M., and Vakakis, A. F., 2018. "Nonreciprocity in the dynamics of coupled oscillators with nonlinearity, asymmetry, and scale hierarchy". *Physical Review E,* ***97***(1), p. 012219.